THE JOURNAL OF PHYSICAL CHEMISTRY C

Article

pubs.acs.org/JPCC

Graphene-Based Planar Nanofluidic Rectifiers

Morteza Miansari,[†,‡] James R. Friend,[†] Parama Banerjee,[§] Mainak Majumder,[§] and Leslie Y. Yeo*[,†]

[†]Micro/Nanophysics Research Laboratory, RMIT University, Melbourne, VIC 3000, Australia

[‡]Department of Mechanical and Aerospace Engineering, Monash University, Clayton, VIC 3800, Australia

[§]Department of Mechanical and Aerospace Engineering, Monash University, Clayton, VIC 3800, Australia

ABSTRACT: Structurally symmetric two-dimensional multilayered graphene oxide films, which facilitate ion transport through "nanochannels" comprising the interstitial spaces between each stacked sheet within the film, are for the first time shown to exhibit peculiar ion current rectification and nonlinear current−voltage characteristics below a critical electrolyte concentration when the interstitial spacing becomes comparable to the Debye screening length such that the film becomes permselective. We attribute the unexpected rectification behavior to the fore−aft asymmetry that arises in the diffusion boundary layer on both sides of the millimeter long film upon reversal between the high resistance positive bias state and the low resistance negative bias state, the asymmetry being primarily a consequence of the trapping and release of counterions within the film, compounded by the nonuniform electric field that occurs in the tortuous nanochannels within the film. In addition to elucidating the influence of the electrolyte concentration and applied bias voltage, we demonstrate the possibility of tuning the ion selectivity and hence the rectification behavior through the solution pH. These first graphene-based nanofluidic rectifiers, which are easily synthesized, therefore offer a flexible, robust, low cost, and facile large-scale alternative to conventional nanochannels that require elaborate and sophisticated nanofabrication.

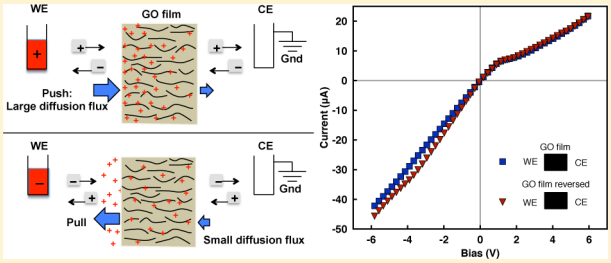

INTRODUCTION

Recent advances in the ability to fabricate nanopores and nanochannels with dimensions comparable to the Debye screening length within which ion concentration polarization effects arise as a consequence of the electrical double-layer confinement[1−3] have led to substantial interest of late in nanofluidic devices.[4,5] Besides providing a convenient platform to mimic and hence investigate the behavior of biological ion channels in physiological processes,[6] the effects of surface properties at the nanoscale[7]—considerably different from that due to their bulk counterpart[8,9]—together with polarization effects in the nanochannel have enabled regulation of transport[10] and biosensing[11−13] down to the single-molecule level, in addition to uncovering new solutions for energy storage and conversion,[14−16] water purification,[17,18] as well as ion concentration and separation.[19,20]

Fundamental to these applications is the ability of the nanochannel or nanopore to regulate ion transport, thus facilitating ion enrichment and depletion and current rectification as a consequence of the ion permselectivity under confinement. Ion enrichment and depletion typically arise at the interface between the nanofluidic channels and the microfluidic reservoirs supplying the channels[1,21,22] as a result of the formation of a diffusion layer enriched with co-ions at the micro-/nano-interface on the entrance side to the nanochannels (the side where the counterions enter) compared with a corresponding counterion depletion region at the exit (the side where counterions leave)[1,3,21] similar to that in nanoporous permselective membranes or granules,[23−25] leading to saturation in the ionic current beyond a critical voltage.[26] Ion current rectification—the ability to conduct ion current preferentially in one direction and inhibit the current flow in the opposite direction when switching the bias voltage, in analogy to a diode[27]—on the other hand—is a consequence of *asymmetry* that exists along the nanochannel, be it in the buffer, surface charge, or geometry.[5]

As a flexible, robust, low cost, and facile large-scale alternative to the complex and cumbersome protocols associated with nanolithography,[28−30] sacrificial layer deposition,[31] and ion[32] or electron beam nanopore milling[33] approaches adopted for the fabrication of nanochannels and nanopores used for ion current rectification, we propose the use of two-dimensional carbon lattice-based (e.g., graphene-based) materials for the fabrication of nanofluidic rectifiers. While ultrafast ion and fluid transport has already been demonstrated in carbon nanotubes (rolled graphene sheets),[17,34−36] offering nearly frictionless flow of water on the graphene surface,[31−33] two-dimensional layered structures of graphene-based materials which possess large surface area (>2600 m^2/g) and superior electronic properties (e.g., electron mobilities >15 000 $cm^2/V{\cdot}s$), on the other hand, offer many opportunities for efficient nanofluidic ion transport.[37] In particular, the massively parallel nanochannel array platform afforded, for example, by restacked exfoliated graphene oxide (GO) sheets[38] allows very high throughput

Received: July 14, 2014
Revised: August 28, 2014
Published: August 29, 2014

   dx.doi.org/10.1021/jp5070006 | *J. Phys. Chem. C* 2014, 118, 21856−21865

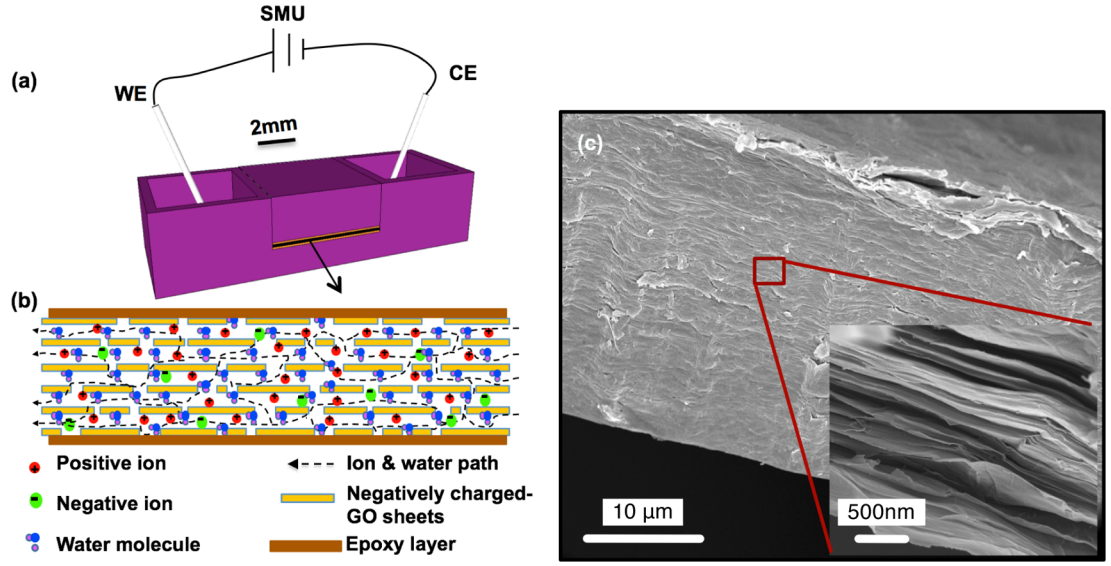

Figure 1. Schematic of (a) the experimental setup and (b) a multilayered GO film, illustrating the possible permeation route: water molecules and ions are transported through a large number of interconnected "nanochannels" formed from the interstitial spaces between the GO sheets.[37,42] WE represents the working electrode and CE the counter electrode. (c) Scanning electron microscopy image of the film cross-section (magnified in the inset) showing the tortuosity of the GO sheets.

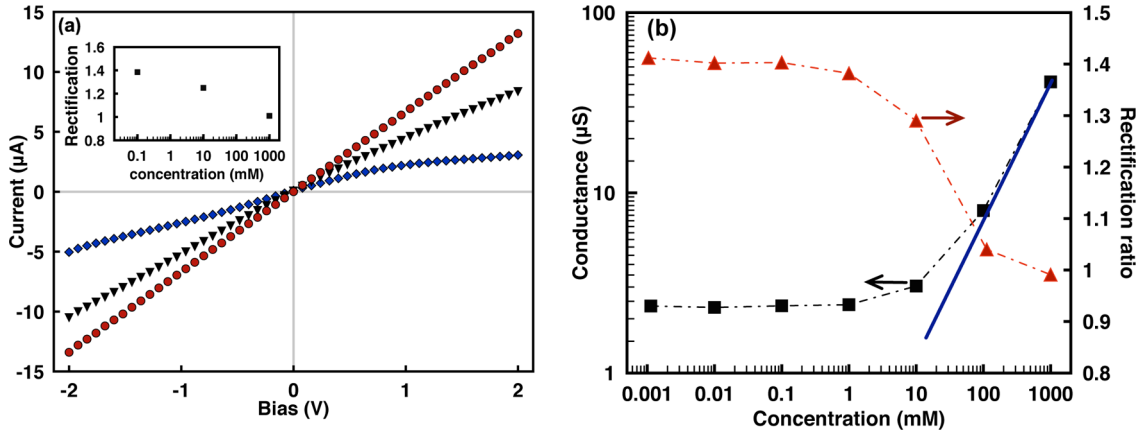

Figure 2. (a) Representative $I-V$ curves for 0.1 mM (diamonds), 10 mM (inverted triangles), and 1000 mM (circles) KCl electrolyte solutions at pH ~ 7. The inset shows the corresponding ion current rectification ratio F which increases together with the nonlinear $I-V$ curves as the ionic strength decreases. (b) Ionic conductance through the GO film (triangles) and the corresponding rectification ratio F (squares) as a function of the KCl electrolyte concentration at pH ~ 7. The dashed lines were added to aid visualization, whereas the solid line represents the bulk conductance.

without the need for elaborate nanofabrication steps while being fairly robust in tolerating high bending strains.[37] Further, the interstitial height of the sheets comprising the film and its surface charge can easily be tuned prior to assembly through the stacking process,[37] the degree of hydration,[39] or intercalation with guest molecules,[40] thus circumventing the need for chemically functionalizing the surfaces of the nanochannel interior. Moreover, the millimeter dimension of the film comprising tens of thousands of interconnected nanoscale fluid "channels" allows them to be conveniently handled and integrated with existing microdevices.[37] As such, these materials have tremendous potential to be exploited for many applications involving nanochannel ion transport such as energy storage,[41] membrane separation,[42] catalysis,[43] and sensing applications.[44]

Nevertheless, despite the recent demonstration of ion transport through the interlayer interstices of these GO films,[37] *nonlinear* current–voltage ($I-V$) characteristics and ion current rectification for nanofluidic diode applications have yet to be reported. Here, we show, for the first time, such characteristics and behavior endowed by the restacked exfoliated GO sheets that make up a structurally symmetric film connecting two fluid reservoirs. Below a critical electrolyte concentration when the Debye screening length becomes comparable to the thickness of the nanoscale interlayer spacing between the GO sheets which are endowed with negative surface charge when dispersed in water due to the attachment of oxygen-containing carboxyl, hydroxyl, and epoxy groups[37,42] during the exfoliation process, the fluid in the interstices becomes polarized, thereby rendering the GO sheets permselective in a manner similar to that which occurs in nanochannels or nanopores. In addition to elucidating the ion current rectification behavior under the influence of various parameters such as the electrolyte concentration and pH, as well as the applied voltage, we postulate a possible mechanism by which the curious rectification behavior arises in the

dx.doi.org/10.1021/jp5070006 | J. Phys. Chem. C 2014, 118, 21856–21865

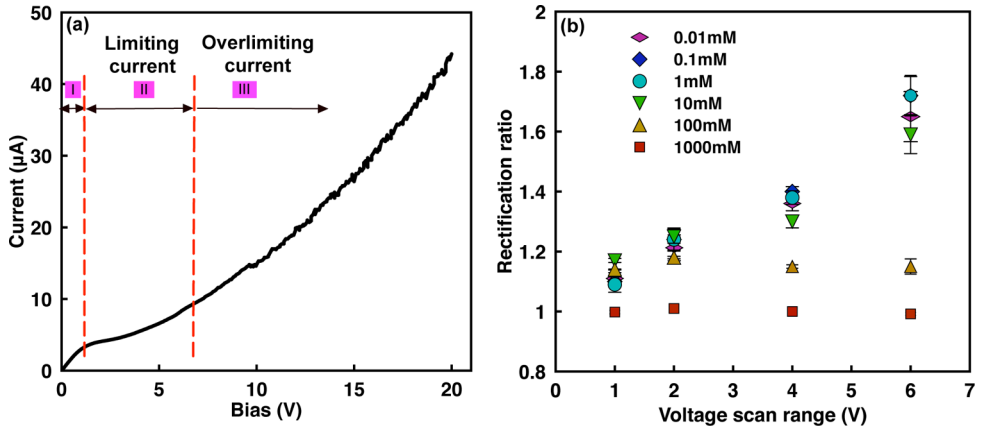

Figure 3. (a) $I-V$ curve measured for 0.1 mM KCl at pH ∼ 7, highlighting the Ohmic (region I), limiting (region II), and overlimiting (region III) current regimes. (b) Rectification ratio F of the GO film at pH ∼ 7 for different KCl electrolyte concentrations over a scan range across −1 to 1 V, −2 to 2 V, −4 to 4 V, and −6 to 6 V. It should be noted that the device employed in obtaining these measurements is different from that used to obtain the results in Figure 2, and hence a slight quantitative variation in the results is observed; qualitatively, however, the behavior associated with both devices is similar.

structurally symmetric film: asymmetry in the profile of the diffusion boundary layers at the entrance and exit of the film, complemented by the natural asymmetry that exists given the nonuniform thickness of the interlayer spacing along the length of the sheets. The fore−aft asymmetry in the diffusion layer profile, in particular, appears to arise as a consequence of ion trapping and release within its sheets and the nonuniform electric field that arises because of the tortuosity of the nanochannels.

RESULTS AND DISCUSSION

Role of Electrolyte Concentration. It is expected that the fluid in the interstices between the GO layers (Figure 1) becomes polarized and hence the GO film rendered permselective when the Debye screening length

$$\kappa^{-1} = (\varepsilon_r \varepsilon_0 RT/2F'^2 C)^{0.5} \quad (1)$$

becomes comparable to the apparent interlayer spacing, estimated to be approximately 1 nm after swelling in water.[37] At standard temperature, and for a relative permittivity ε_r of 4.6 for KCl, this occurs when the electrolyte concentration C is below approximately 100 mM; in eq 1, ε_0 is the permittivity of free space, R the molar gas constant, and F' the Faraday constant. Given the negatively charged surfaces of the GO sheets,[37,42] the transport of co-ions (Cl^- anions) is thus excluded from the interstitial spaces between the GO sheets due to electrostatic repulsion, thus selectively permitting only the passage of the counterions (K^+ cations) below this critical concentration for a given average interlayer spacing.[38,45] This can be seen by the representative $I-V$ curves and the associated conductance measurements in Figure 2, wherein the conductance in the film begins to deviate from that of the bulk below the critical electrolyte concentration due to the higher cation concentration in the interstitial spaces of the film compared with the bulk as a consequence of the permselectivity. The conductance plateaus concomitantly below the critical concentration and becomes independent of the electrolyte concentration, characteristic of surface-charge dominant ion transport through polarized nanochannels.[37]

This can be seen more clearly from the following relationship for the conductance of a single nanochannel, comprising contributions from the bulk and the double layer conductances[37,45,46]

$$G = [e(\mu_{K^+} + \mu_{Cl^-})CN_A wh/l] + [2\mu_{K^+}\sigma_s w/l] \quad (2)$$

wherein e is the elementary charge; μ_{K^+} and μ_{Cl^-} are the cation and anion mobilities, respectively; N_A is Avogadro's constant; σ_s is the surface charge density; w and l are the width and length of the film, respectively; and h is the spacing between neighboring GO sheets. It can thus be seen that the first term, which represents the bulk conductance, dominates at high ionic concentrations when the surface charges are mostly screened, whereas the second term, which represents the double-layer conductance, dominates at low ionic strength; hence, the nanochannel conductance becomes independent of both the nanochannel height and the bulk concentration, i.e., the ion transport is controlled by the surface charges. In any case, as with Raidongia and Huang,[37] microampere currents are observed, which are significantly larger than that typically measured in nanofluidic channel arrays[47−49] but, even more remarkably, with millimeter-long films instead of the centimeter-long films reported by Raidongia and Huang.[37]

Nevertheless, the permselectivity of the GO film, while a necessary condition, is insufficient in itself to explain the ion current rectification behavior we observe in Figure 2 (captured, in particular, by the ion current rectification ratio F, which is defined as the ratio of the currents measured for applied voltages with the same amplitude but opposite polarities $|I_{(-V)}/I_{(+V)}|$, where $I_{(-V)}$ and $I_{(+V)}$ are, respectively, the reverse and forward currents measured at negative and positive bias voltages applied to the working electrode (WE) below the critical concentration, at least for the *structurally symmetric* films examined here. This is because the film permselectivity exhibits mirror fore−aft symmetry, given that the polarization reverses when the applied bias voltage is reversed. Rather, we postulate that the film possesses certain asymmetrical characteristics that, together with its permselectivity, constitute the requisite conditions necessary for ion current rectification in the film, the rectification behavior increasing the more permselective the film as the ionic concentration decreases, as observed in Figure 2b. A possible source of such asymmetry in the film, necessary for it to exhibit ion current rectification behavior, is discussed in the following section.

dx.doi.org/10.1021/jp5070006 | J. Phys. Chem. C 2014, 118, 21856−21865

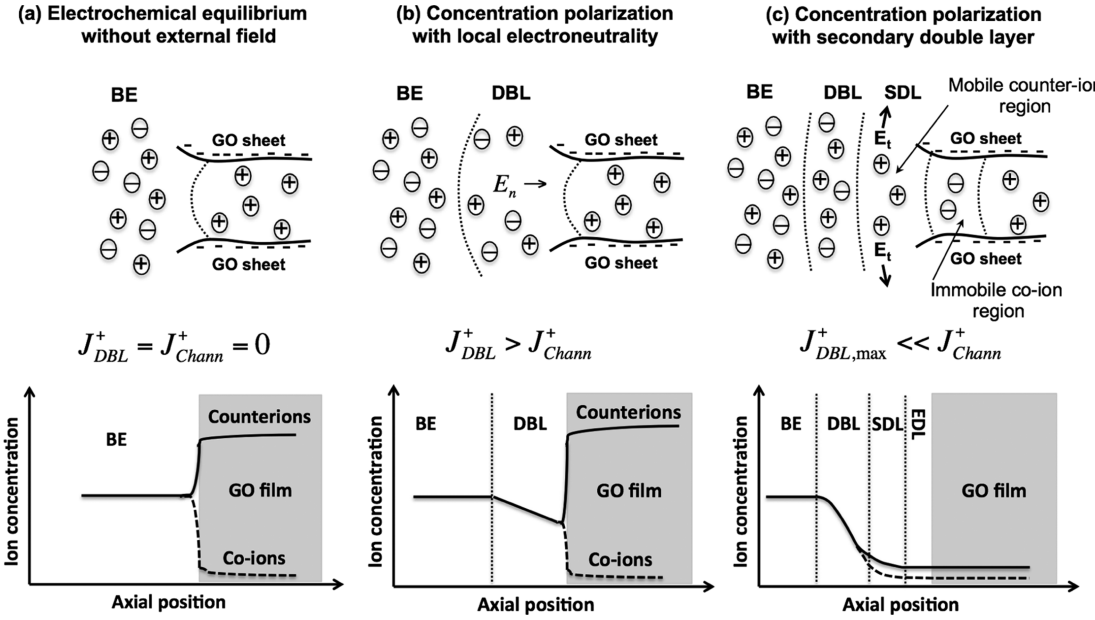

Figure 4. (Top) Schematic illustration of the entrance of the permselective GO film and (bottom) the corresponding concentration distribution profiles there. (a) Electrochemical equilibrium in the absence of an external applied electric field. (b) Concentration polarization with a locally electroneutral diffusion boundary layer (DBL); here, the cation flux density within the nanochannels J^+_{chann} is small compared to the flux density J^+_{DBL} in the diffusion boundary layer. (c) At higher bias voltages above the gating voltage, J^+_{chann} exceeds J^+_{DBL}, giving rise to a secondary double layer (SDL). BE represents the bulk electrolyte and EDL the electrical double layer; E_n and E_t denote the normal and tangential components of the applied electric field, respectively. Adapted from ref 61.

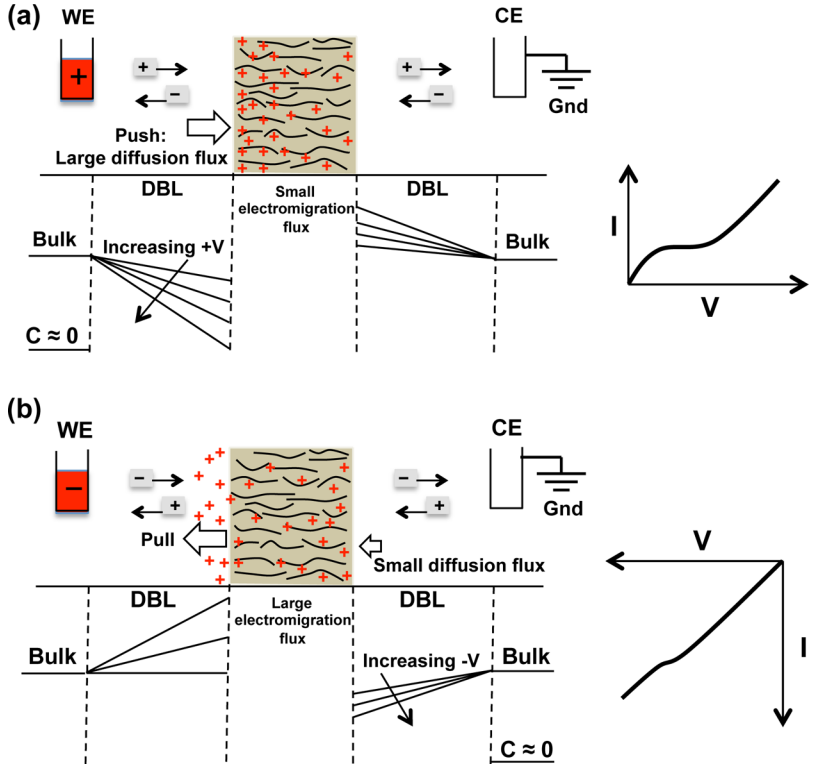

Figure 5. Schematic illustration of the differing dominant ion transport mechanisms (PUSH vs PULL) and the resulting ion concentration distributions in the diffusion boundary layer (DBL) on both the entrance and exit of the cation-selective GO film for (a) the high resistance positive (0 to $+V$) bias state applied to the WE in which ion trapping within the GO sheets occurs and (b) the low resistance negative (0 to $-V$) bias state applied to the WE in which trapped ions are released from within the GO sheets. The representative $I-V$ curves for both states are also shown on the right. Note the asymmetry in the diffusion boundary layer in which the counterions in the diffusion boundary layer at the exit are not completely depleted in the low resistance negative bias state (b) compared to that at the entrance and thus the absence of significant saturation in the current in the corresponding $I-V$ curve.

dx.doi.org/10.1021/jp5070006 | J. Phys. Chem. C 2014, 118, 21856−21865

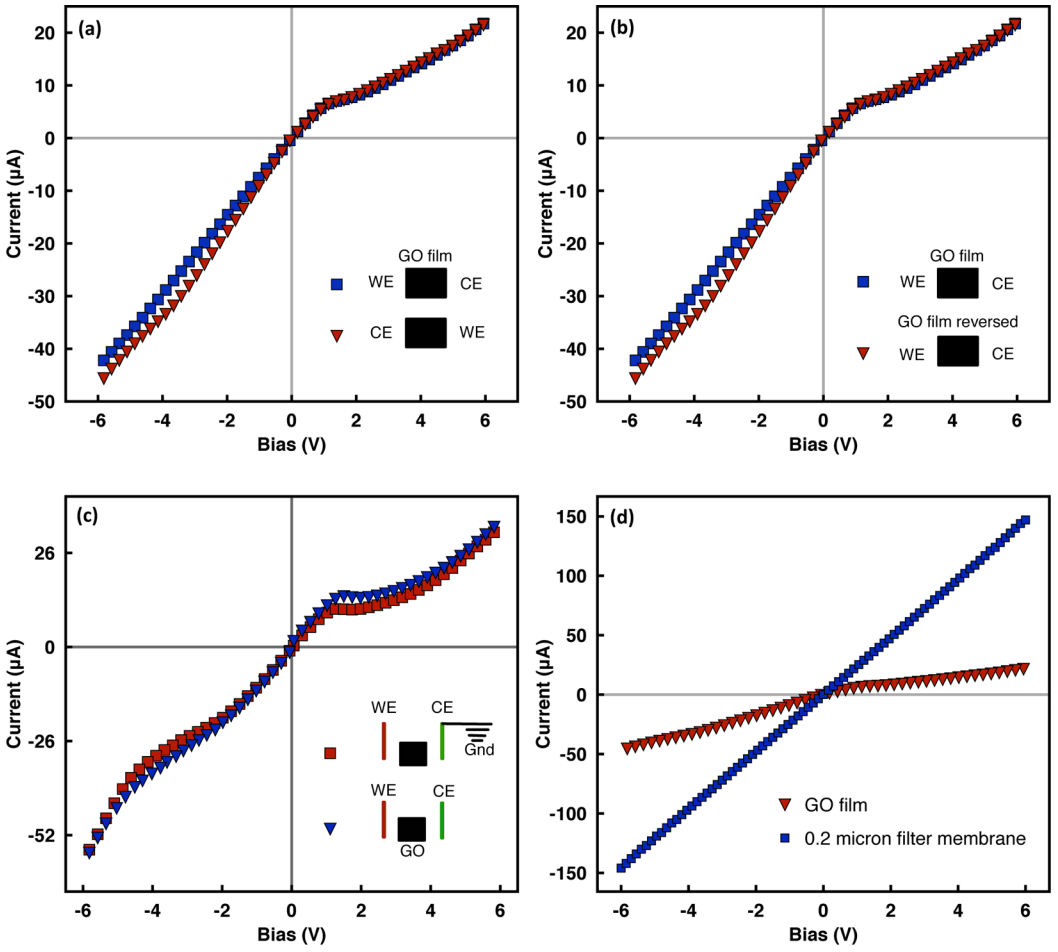

Figure 6. No significant differences are observed in the $I-V$ characteristics for 0.1 mM KCl at pH ~ 7 when (a) the WE and CE on both sides of the film (Figure 5) are swapped, (b) the ends of the GO film are reversed while leaving the WE and CE unchanged, and (c) the CE is grounded. Instead, only very small differences are observed, which can be attributed to weak asymmetry arising from inherent defects or contamination in the GO film or uneven electrochemical reactions between the electrodes. The statistical differences were analyzed using a one-way ANOVA test given that the data were normally distributed and demonstrated homogeneity of variance, as determined from Levene's test; results were considered significant if $p < 0.05$. (d) Replacing the GO film with a 0.2 μm filter membrane leads to the suppression of the rectification effect; the linear $I-V$ curves for the mock film comprising the filter membrane provide further evidence that the asymmetric effects leading to the rectification behavior in the GO film do not originate externally from the electronics, instrumentation, or connections.

Effect of the Applied Bias Voltage. The effect of the applied bias voltage on the system and the ion current rectification can be seen in Figure 3. In contrast to that observed by Raidongia and Huang,[37] who only considered small bias voltage ranges, it can be seen that the system exhibits similar $I-V$ characteristics to that typically observed in permselective nanochannels[3,21,26,50−56] wherein three distinct regimes are apparent. At low voltages, the usual linear Ohmic dependence on voltage exists (region I in Figure 3a) in which the bulk conductance term in eq 2 dominates similar to that observed when permselectivity in the channel is lost when the ionic concentration is above the critical value. The bulk Ohmic resistance arises here due to the charge buildup and hence the concentration gradient that arises at the film−reservoir entrance interface (on the side of the WE) due to the film permselectivity, the local electroneutrality of this counterion-depleted polarization layer being primarily responsible for the Ohmic behavior.[23] The concentration gradient then stipulates that ion transport within the sheets in the film is limited by diffusion through this layer.[54] Given that the conductance in the low-voltage Ohmic region is finite and does not scale linearly with the bulk electrolyte concentration (Figure 3b), the Ohmic resistance is then not due to the external resistance alone but also due to the differential resistance across the film. In other words, the convergence of the electric field from the bulk into the nanoscale confinement imposed by the film gives rise to a large logarithmically singular current density, which can only be sustained by the diffusion layer.[26]

Above a threshold voltage (around 1 V in this case), this differential resistance increases to a large, finite value, and the current saturates (region II in Figure 3a) to a level known as the limiting current density when the ion concentration at the film−reservoir entrance interface vanishes.[57] The bottleneck in the current flux then moves upstream from the film to the bulk. Beyond a further voltage known as the critical gating voltage (approximately 6 V in this case), the differential resistance once again decreases to become comparable to that in the bulk Ohmic region. This overlimiting current region[58] (region III in Figure 3a) arises because the large applied voltages drive a strong electromigration flux through the interstitial space of the GO sheets that overcomes the diffusive flux into the sheets through the polarization layer such that local electroneutrality breaks down and an immobile layer of co-ions (i.e., the Cl^- anions) forms at the entrance to the film together with a

dx.doi.org/10.1021/jp5070006 | J. Phys. Chem. C 2014, 118, 21856−21865

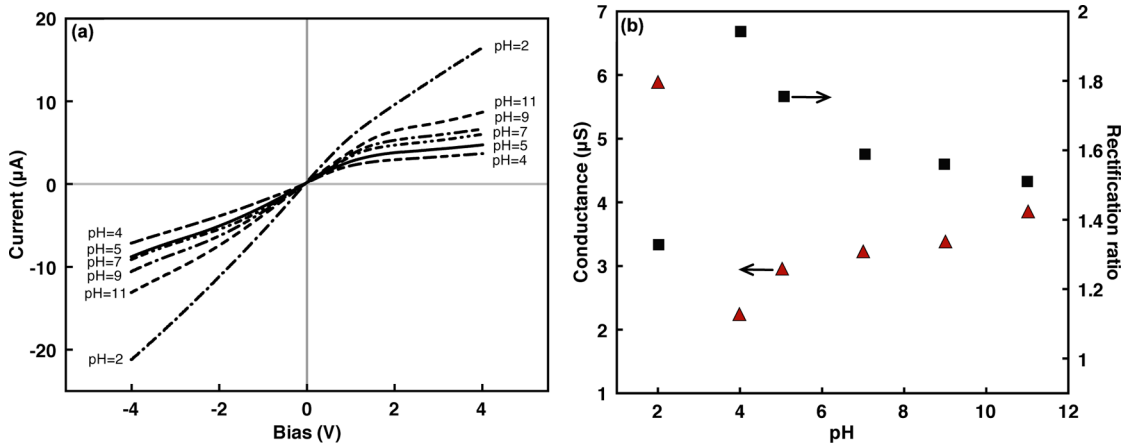

Figure 7. (a) $I-V$ characteristics recorded for the GO film at different pH values for a 0.1 mM KCl electrolyte solution. (b) Dependence of the conductance (triangles) and rectification ratio F at ±4 V (squares) on the pH of the KCl solution, which was adjusted through the addition of HCl and KOH.

secondary double layer comprising a counterion-enriched region (see Figure 4).

We postulate that it is the asymmetry in the diffusion boundary layers at the entrance and exit of the film illustrated in Figure 4 that is responsible for the ion current rectification behavior observed in Figure 2. This is due in part to the polarity of the bias potential applied to the WE as illustrated in Figure 5. Counterions are repelled from the electrode when a positive bias is applied to the WE, giving rise to the diffusion boundary layer given the requirement of local electroneutrality at the entrance interface to the polarized film. This diffusion boundary layer then controls the ion transport through the film beyond the threshold voltage discussed above given the bottleneck that exists in the electromigration flux through the sheets, compounded by the increase in the resistance within the sheets arising from the tortuosity of the nanochannels that make up the interstitial spaces between the sheets and the tendency for counterion transport to be retarded due to ion trapping effects by the surface oxides present on the GO sheets, which are strong polar sites that adsorb water molecules.[59,60] In other words, a PUSH mechanism exists in which electrolyte migration through the sheets is retarded (Figure 5a). Consequently, the current saturates when the positive bias voltage exceeds the threshold voltage, as shown in Figure 2a. On the other hand, when a negative bias is applied to the WE, a PULL mechanism exists where counterions through the cation-selective sheets are drawn to the WE, thus releasing the counterions from their trapped state within the sheets. In this case, a large electromigration flux ensues, alleviating the bottleneck in ion transport through the GO sheets, resulting in a decrease in the resistance across the film. As illustrated in Figure 5b, the counterion concentration in the diffusion boundary layer at the film exit is therefore controlled by this drift and does not deplete completely, evidenced by the absence of the saturation in the ion current even when the negative bias voltage exceeds the threshold value (Figure 2a).

It is therefore reasonable that this fore−aft asymmetry in the diffusion layer beyond the threshold voltage, i.e., the reversal between the high resistance positive bias state to the low resistance negative bias state, is responsible for the ion current rectification behavior of the GO film. This is confirmed by the observation that the rectification factor is enhanced the further the departure from the linear Ohmic behavior as the applied bias voltage is increased (Figure 3b) and by the absence of any noticeable difference in the $I-V$ characteristics when the WE and CE ends are swapped (Figure 6a) or when both sides of the GO film are reversed while keeping the WE and CE ends unchanged (Figure 6b). To ensure that the CE is truly at zero potential instead of negative (or positive) when a positive (or negative) bias is applied to the WE in which case symmetry in the diffusion boundary layers at the entrance and exit of the film would ensue (i.e., the PUSH mechanism occurs on one end, and the PULL mechanism occurs concurrently at the other, and vice versa), we also carried out an additional measurement in which we directly grounded the CE (Figure 6c). Further, we also reversed the cables as well as the terminals to the SMU in a set of additional experiments to verify that the asymmetry did not originate from other sources, i.e., the electronics, external to the film; again, we did not observe any significant differences in the rectification behavior, which we note was reproducible over the number of repeats (between three to five times, at least) in the measurements (not shown). That no significant difference is again observed in the $I-V$ characteristics then lends further support to our postulated mechanism above of asymmetry in the diffusion boundary layers at the film entrance and exit (Figure 4). Finally, we also conducted a control experiment in which the entire setup was replicated but in a mock film consisting of a filter membrane with comparable pore size mounted in a U-shaped electrochemical cell. In this case, however, linear $I-V$ curves without rectification were observed, again confirming that the asymmetry did not originate from the electronic equipment, instrumentation, and connections (Figure 6d).

It is possible that the rectification behavior was not observed in previous studies of these GO films[37] because the threshold voltage was never exceeded. It is also possible that these effects are compounded by the inherent asymmetry of the film: we note that the graphene oxidation process typically introduces microscopic voids or stacking faults in the sheets.[37] While these did not measurably affect the overall permselective characteristics and hence the surface-charge-driven ion transport through the sheets, as long as the defects are not spread along the direction of the ionic current,[37] it is likely that such defects, together with the nonuniformity in the interlayer spacing (see, for example, the SEM images in Figure 1c), could increase the ion trapping propensity within the sheets and form a fore−aft

dx.doi.org/10.1021/jp5070006 | J. Phys. Chem. C 2014, 118, 21856−21865

asymmetry in the film that further enhances the rectification behavior reported here (Figure 2), albeit to a much lesser extent (Figure 6a). Further, a small degree of asymmetry could also have been introduced to the film when its ends are cut and exposed for subsequent connection to the reservoirs, although rectification effects arising from such appear to be negligible (Figure 6b).

Influence of the Electrolyte pH. Figure 7 illustrates the dependence of the conductance through the GO film and hence its $I-V$ characteristics and rectification behavior on the pH of the electrolyte solution. Although the overall dependence on the solution pH seen is as would be expected given that the surface charge along the GO sheets can be modified by changing the pH, the observed maximum in the rectification factor at a pH value of around 4 is less intuitive. This critical value appears to coincide with the value of the acid dissociation constant pK_a of approximately 4.2 for carboxyl groups, at which the dissociation of the carboxylic acid groups in the GO sheets occurs

$$COOH \rightleftharpoons COO^- + H^+$$

At large pH values above this critical value, the reduction in H^+ concentration leads to the dissociation of carboxylic acid, which, in turn, causes an increase in the surface charge density of the COO^- groups on the GO sheets. Consequently, the GO sheets carry the maximum unscreened negative surface charges that attract counterions from the bulk into the interstitial spaces between the sheets, giving rise to an increase in the double-layer conductance (Figure 7b). Thus, the conductance is expected to decrease with decreasing pH until the dissociation point of carboxyl groups (p$K_a \sim 4.2$) is reached, where the vanishing COO^- surface groups along the surface of the GO sheets lead to a reduction in the surface charge and hence the electrostatic repulsion associated with the overlapping of double layers in nanochannels, resulting in the collapse of the film into aggregated sheets.[62−64] As a consequence of the concomitant decrease in the number of stacked "nano-channels", there is a dip in the total conductance, which is the conductance of a single channel multiplied by the number of channels, as observed in Figure 7b. The collapse of the film, nevertheless, increases the permselectivity due to the decrease in the interstitial spacing between the negatively charged aggregated sheets, thus enhancing the rectification in a manner to that similar to decreasing ionic concentration (see the section on the Role of Electrolyte Concentration). As such, maximum rectification is observed at the critical pH value of around 4 (Figure 7). This maximum around the critical pH can be seen more clearly in Figure 8 wherein the rectification is enhanced at higher bias voltages.

We note that the dissociation of other groups present on the GO sheets also contributes to the observed rectification behavior, albeit to a lesser extent. For example, hydroxyl and phenolic groups on the GO sheets tend to dissociate at a pK_a value of around 6.6 and 9.8,[62] respectively, contributing to the slight decrease in the surface charge density and hence the conductance as the pH is reduced from 11 to 5. Furthermore, there is an increase in the rectification factor due to similar decreases in the interstitial spacing and hence increases in the permselectivity. The increase in the H^+ concentration as the pH is reduced below 4 drives a further reduction in the surface charge density, consistent with observations of a sharp decrease in measurements of the zeta potential of GO sheets in other work.[62−64] However, the conductance is seen to increase

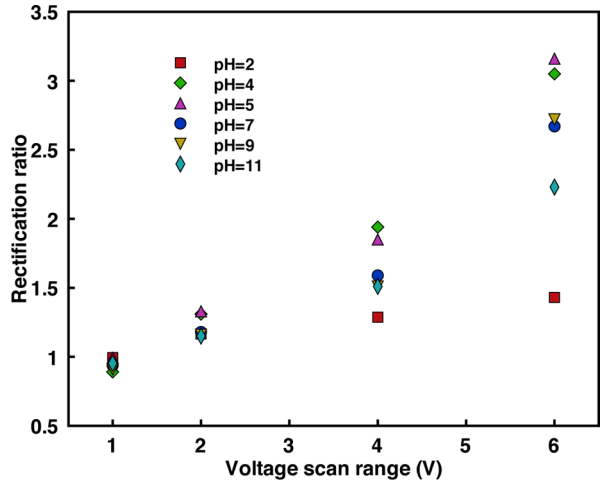

Figure 8. pH dependence of the rectification ratio F of the GO film for a 0.1 mM KCl solution with a scan range from −1 to 1 V, −2 to 2 V, −4 to 4 V, and −6 to 6 V.

sharply with a large corresponding drop in the rectification factor, in contrast to that observed above at pH ∼ 4. This anomaly can be explained by both the increase in the electrolyte concentration and the increase in protonation within the GO sheets when HCl is added to lower the pH (again, see the section on the Role of Electrolyte Concentration). The protons, which inherently have greater mobility than the cations, are thus responsible for a significant proton current that contributes to the large increase in the overall conductance.

CONCLUSION

We demonstrate, for the first time, the nonlinear current−voltage characteristics and ion current rectification behavior in the "nanochannels" formed in the interstices of multilayered graphene oxide films. While permselectivity of the film—arising when the Debye screening length becomes comparable to the interstitial spacing of the sheets below a critical electrolyte concentration—is a necessary condition for the film's rectification behavior, and increasing permselectivity is shown to increase the rectification factor, it alone is however insufficient to give rise to the rectification given the structural symmetry of the film. Fore−aft asymmetry is instead also a necessary condition for rectification—such asymmetry arising in the structurally symmetric GO film primarily in the diffusion boundary layers at the entrance and exit ends of the film due to the reversal between the high resistance positive bias state and the low resistance negative bias state of the film, compounded by effects of ion trapping/release as well as electric field nonuniformity in the tortuous nanochannels that comprise the film. It is also possible that defects in the film introduced during the synthesis and fabrication process such as voids in the surface functional groups, stacking faults, or nonuniformity in the interstitial spaces that make up the nanochannels between the stacked sheets comprising the two-dimensional film further contribute to the rectification by enhancing ion trapping as well as the film's asymmetry.

The solution pH is also shown to strongly influence surface charging along the graphene oxide sheets and hence the conductance and the rectification behavior of the film. In particular, maximum rectification is observed at the acid dissociation point when the diminution of the surface charge

dx.doi.org/10.1021/jp5070006 | J. Phys. Chem. C 2014, 118, 21856−21865

along the sheets leads to their aggregation with the collapse of the double layer and thus the film. Rectification can further be enhanced by decreasing the ionic concentration in the bulk as the permselectivity of the film increases or by increasing the applied bias voltage. Together with the low cost, ease, and simplicity of synthesizing, chemically functionalizing, handling, integrating, and scaling up these films for use in practical microdevices, the ultrahigh throughput afforded by the massively parallel "nanochannel" arrays formed by the interstitial spaces between the graphene oxide sheets makes these films an extremely attractive alternative to nanofluidic rectification devices for a broad range of applications spanning biosensing, energy storage, membrane separation, and beyond.

METHODS

Synthesis of Graphene Oxide Films. The multilayered GO films were prepared by vacuum filtration of a chemically exfoliated GO dispersion (modified Hummer's method[41,65]). To prepare the freestanding film, 100 mL of 0.05 wt % GO solution was filtered through a cellulose acetate filter membrane (47 mm diameter, 0.2 μm pore size; Whatman Ltd., Maidstone, UK). The GO film was then air-dried and peeled off from the filter membrane and cut using a blade into the desirable dimension, in this case, a 3 mm × 3 mm rectangular film, whose thickness was measured using a digital micrometer caliper; at least five different locations were measured, and the averaged thickness was found to be approximately 30 μm. The top and bottom surfaces of the films were subsequently covered with a layer of UV epoxy and immediately exposed to the UV light to avoid leakage such that the fluid transport occurs solely through the interlayer spacing of the GO film. The film was then sandwiched between two polydimethylsiloxane (PDMS) layers using plasma bonding. The nanofluidic device was finally accomplished by connecting the ends of the film to two reservoirs filled with electrolyte solution (Figure 1); for most of the experiments, this comprised chloride solutions (KCl) with different pH and ionic strength.

Characterization. Two Ag/AgCl reference electrodes were inserted into each half-cell solution, and the $I-V$ curves associated with the ion transport through the GO layers were recorded using a sourcemeter unit (SMU; model 6430, Keithley Instruments Inc., Cleveland, OH) placed inside a Faraday cage. For the investigation of the pH dependence, the reservoirs were filled with 0.1 mM KCl at different pH, which was adjusted through the addition of potassium hydroxide (KOH) or hydrochloric acid (HCl). Cross-sectional images along the long axis of the films were also obtained using scanning electron microscopy (Nova NanoSEM 450, FEI, Hillsboro, OR).

To ensure that the source of the rectification observed is not external to the film, we carried out a series of additional control experiments in which the electrodes, the film itself, as well as the electronics, i.e., the cables and terminals into the SMU and the SMU itself, were reversed. In addition, the entire setup used for the current measurements was replicated in a mock film by recording the ionic current through a filter membrane with 0.2 μm pore size mounted in a U-shaped electrochemical cell. In all cases, experiments were repeated at least three to five times to ensure reproducibility in the observed rectification effect. Further, to eliminate the possibility of the asymmetry originating due to the solutions external to the film, we ensured—prior to the measurements—that the film was fully hydrated and swelled by filling both reservoirs with DI water for approximately 2 days after which they were filled with the electrolytes at the requisite concentrations and maintained for a further 12 h. The electrical conductance of the nanochannels was then calculated every 1 h to obtain the $I-V$ curves until no detectable changes were observed; i.e., steady state was attained while ensuring that the film remained fully wetted.

AUTHOR INFORMATION

Corresponding Author

*E-mail: leslie.yeo@rmit.edu.au.

Notes

The authors declare no competing financial interest.

ACKNOWLEDGMENTS

LYY is funded through an Australian Research Council (ARC) Future Fellowship (FT130100672) as well as Discovery Project grant DP0985253. JRF is grateful for support of this work from Discovery Project grants DP120100013 and DP120100835, the Melbourne Centre for Nanofabrication for a Senior Tech Fellowship, and RMIT University for the Vice-Chancellor's Senior Research Fellowship. This work was performed in part at the Melbourne Centre for Nanofabrication (MCN), which is the Victorian Node of the Australian National Fabrication Facility (ANFF).

REFERENCES

(1) Chang, H. C.; Yossifon, G. Understanding electrokinetics at the nanoscale: A perspective. *Biomicrofluidics* **2009**, *3*, 012001.
(2) Stein, D.; Kruithof, M.; Dekker, C. Surface-charge-governed ion transport in nanofluidic channels. *Phys. Rev. Lett.* **2004**, *93*, 035901.
(3) Kim, S. J.; Wang, Y. C.; Lee, J. H.; Jang, H.; Han, J. Concentration polarization and nonlinear electrokinetic flow near a nanofluidic channel. *Phys. Rev. Lett.* **2007**, *99*, 044501.
(4) Sparreboom, W.; Van den Berg, A.; Eijkel, J. C. Principles and applications of nanofluidic transport. *Nat. Nanotechnol.* **2009**, *4*, 713–720.
(5) Zhou, K.; Perry, J. M.; Jacobson, S. C. Transport and Sensing in Nanofluidic Devices. *Annu. Rev. Anal. Chem.* **2011**, *4*, 321–341.
(6) Hille, B. *Ion Channels of Excitable Membranes*, 3rd ed.; Sinauer: Sunderland, 2001.
(7) Logan, B. E.; Elimelech, M. Membrane-based processes for sustainable power generation using water. *Nature* **2012**, *488*, 313–319.
(8) Van den Berg, A.; Craighead, H. G.; Yang, P. From microfluidic applications to nanofluidic phenomena. *Chem. Soc. Rev.* **2010**, *39*, 899–900.
(9) Bocquet, L.; Charlaix, E. Nanofluidics, from bulk to interfaces. *Chem. Soc. Rev.* **2010**, *39*, 1073–1095.
(10) Karnik, R.; Castelino, K.; Majumdar, A. Field-effect control of protein transport in a nanofluidic transistor circuit. *Appl. Phys. Lett.* **2006**, *88*, 123114.
(11) Kasianowicz, J. J.; Brandin, E.; Branton, D.; Deamer, D. W. Characterization of individual polynucleotide molecules using a membrane channel. *Proc. Natl. Acad. Sci. U.S.A.* **1996**, *93*, 13770–13773.
(12) Dekker, C. Solid-state nanopores. *Nat. Nanotechnol.* **2007**, *2*, 209–215.
(13) Vlassiouk, I.; Kozel, T. R.; Siwy, Z. S. Biosensing with nanofluidic diodes. *J. Am. Chem. Soc.* **2009**, *131*, 8211–8220.
(14) Daiguji, H.; Yang, P.; Szeri, A. J.; Majumdar, A. Electrochemomechanical energy conversion in nanofluidic channels. *Nano Lett.* **2004**, *4*, 2315–2321.
(15) Kim, D. K.; Duan, C.; Chen, Y. F.; Majumdar, A. Power generation from concentration gradient by reverse electrodialysis in ion-selective nanochannels. *Microfluid. Nanofluid.* **2010**, *9*, 1215–1224.
(16) Moghaddam, S.; Pengwang, E.; Jiang, Y. B.; Garcia, A. R.; Burnett, D. J.; Brinker, C. J.; Masel, R. I.; Shannon, M. A. An

inorganic−organic proton exchange membrane for fuel cells with a controlled nanoscale pore structure. *Nat. Nanotechnol.* **2010**, *5*, 230−236.
(17) Holt, J. K.; Park, H. G.; Wang, Y.; Stadermann, M.; Artyukhin, A. B.; Grigoropoulos, C. P.; Noy, A.; Bakajin, O. Fast mass transport through sub-2-nanometer carbon nanotubes. *Science* **2006**, *312*, 1034−1037.
(18) Kim, S. J.; Ko, S. H.; Kang, K. H.; Han, J. Direct seawater desalination by ion concentration polarization. *Nat. Nanotechnol.* **2010**, *5*, 297−301.
(19) Kim, S. J.; Song, Y. A.; Han, J. Nanofluidic concentration devices for biomolecules utilizing ion concentration polarization: theory, fabrication, and applications. *Chem. Soc. Rev.* **2010**, *39*, 912−922.
(20) Piruska, A.; Gong, M.; Sweedler, J.; Bohn, P. W. Nanofluidics in chemical analysis. *Chem. Soc. Rev.* **2010**, *39*, 1060−1072.
(21) Yossifon, G.; Chang, H.-C. Selection of nonequilibrium overlimiting currents: universal depletion layer formation dynamics and vortex instability. *Phys. Rev. Lett.* **2008**, *101*, 254501.
(22) Holtzel, A.; Tallarek, U. Ionic conductance of nanopores in microscale analysis systems: Where microfluidics meets nanofluidics. *J. Sep. Sci.* **2007**, *30*, 1398−1419.
(23) Dukhin, S. S. Electrokinetic phenomena of the second kind and their applications. *Adv. Colloid Interface Sci.* **1991**, *35*, 173−196.
(24) Leinweber, F. C.; Tallarek, U. Concentration polarization-based nonlinear electrokinetics in porous media: induced-charge electro-osmosis. *J. Phys. Chem. B* **2005**, *109*, 21481−21485.
(25) Wang, S.-C.; Wei, H.-H.; Chen, H. P.; Tsai, M. H.; Yu, C. C.; Chang, H. C. Dynamic superconcentration at critical-point double-layer gates of conducting nanoporous granules due to asymmetric tangential fluxes. *Biomicrofluidics* **2008**, *2*, 014102.
(26) Yossifon, G.; Mushenheim, P.; Chang, Y. C.; Chang, H. C. Nonlinear current−voltage characteristics of nanochannels. *Phys. Rev. E* **2009**, *79*, 046305.
(27) Cheng, L.-J; Guo, L. J. Nanofluidic diodes. *Chem. Soc. Rev.* **2010**, *39*, 923−938.
(28) Kim, S. H.; Cui, Y.; Lee, M. J.; Nam, S. W.; Oh, D.; Kang, S. H.; Kim, Y. S.; Park, S. Simple fabrication of hydrophilic nanochannels using the chemical bonding between activated ultra-thin PDMS layer and cover glass by oxygen plasma. *Lab Chip* **2011**, *11*, 348−353.
(29) Hibara, A.; Saito, T.; Kim, H. B.; Tokeshi, M.; Ooi, T.; Nakao, M.; Kitamori, T. Nanochannels on a fused-silica microchip and liquid properties investigation by time-resolved fluorescence measurements. *Anal. Chem.* **2002**, *74*, 6170−6176.
(30) Tong, H. D.; Jansen, H. V.; Gadgil, V. J.; Bostan, C. G.; Berenschot, E.; Rijn, C. J. M. V.; Elwenspoek, M. Silicon nitride nanosieve membrane. *Nano Lett.* **2004**, *4*, 283−287.
(31) Abgrall, P.; Nguyen, N. T. *Nanofluidics*; Artech House: Boston, 2009.
(32) Li, J.; Stein, D.; McMullan, C.; Branton, D.; Aziz, M. J.; Golovchenko, J. A. Ion-beam sculpting at nanometre length scales. *Nature* **2001**, *412*, 166−169.
(33) Storm, A. J.; Chen, J. H.; Ling, X. S.; Zandbergen, H. W.; Dekker, C. Fabrication of solid-state nanopores with single-nanometre precision. *Nat. Mater.* **2003**, *2*, 537−540.
(34) Majumder, M.; Chopra, N.; Andrews, R.; Hinds, B. J. Nanoscale hydrodynamics: Enhanced flow in carbon nanotubes. *Nature* **2005**, *438*, 44.
(35) Whitby, M.; Cagnon, L.; Thanou, M.; Quirke, N. Enhanced fluid flow through nanoscale carbon pipes. *Nano Lett.* **2008**, *8*, 2632−2637.
(36) Liu, H.; He, J.; Tang, J.; Liu, H.; Pang, P.; Cao, D.; Krstic, P.; Joseph, S.; Lindsay, S.; Nuckolls, C. Translocation of single-stranded DNA through single-walled carbon nanotubes. *Science* **2010**, *327*, 64−67.
(37) Raidongia, K.; Huang, J. Nanofluidic ion transport through reconstructed layered materials. *J. Am. Chem. Soc.* **2012**, *134*, 16528−16531.
(38) Siwy, Z.; Gu, Y.; Spohr, H. A.; Baur, D.; Wolf-Reber, A.; Spohr, R.; Apel, P.; Korchev, Y. E. Rectification and voltage gating of ion currents in a nanofabricated pore. *Europhys. Lett.* **2002**, *60*, 349−355.
(39) Lerf, A.; Buchsteiner, A.; Pieper, J.; Schottl, S.; Dekany, I.; Szabo, T.; Boehm, H. P. Hydration behavior and dynamics of water molecules in graphite oxide. *J. Phys. Chem. Solids* **2006**, *67*, 1106−1110.
(40) Stankovich, S.; Dikin, D. A.; Compton, O. C.; Dommett, G. H. B.; Ruoff, R. S.; Nguyen, S. T. Systematic post-assembly modification of graphene oxide paper with primary alkylamines. *Chem. Mater.* **2010**, *22*, 4153−4157.
(41) Stoller, M. D.; Park, S.; Zhu, Y.; An, J.; Ruoff, R. S. Graphene-based ultracapacitors. *Nano Lett.* **2008**, *8*, 3498−3502.
(42) Paul, D. R. Creating new types of carbon-based membranes. *Science* **2012**, *335*, 413−414.
(43) Machado, B. F.; Serp, P. Graphene-based materials for catalysis. *Catal. Sci. Technol.* **2012**, *2*, 54−75.
(44) Shao, Y.; Wang, J.; Wu, H.; Liu, J.; Aksay, I. A.; Lin, Y. Graphene based electrochemical sensors and biosensors: a review. *Electroanalysis* **2010**, *22*, 1027−1036.
(45) Schoch, R. B.; Renaud, P. Ion transport through nanoslits dominated by the effective surface charge. *Appl. Phys. Lett.* **2005**, *86*, 253111−253113.
(46) Cheng, L. J.; Guo, L. Rectified ion transport through concentration gradient in homogeneous silica nanochannels. *Nano Lett.* **2007**, *7*, 3165−3171.
(47) Fan, R.; Huh, S.; Yan, R.; Arnold, J.; Yang, P. Gated proton transport in aligned mesoporous silica films. *Nat. Mater.* **2008**, *7*, 303−307.
(48) Duan, C.; Majumdar, A. Anomalous ion transport in 2-nm hydrophilic nanochannels. *Nat. Nanotechnol.* **2010**, *5*, 848−852.
(49) Wu, J.; Gerstandt, K.; Zhang, H.; Hinds, B. J. Electrophoretically induced aqueous flow through single-walled carbon nano-tube membranes. *Nat. Nanotechnol.* **2012**, *7*, 133−139.
(50) Mishchuk, N. A.; Takhistov, P. V. Electroosmosis of the second kind. *Colloid Surf. A* **1995**, *95*, 119−131.
(51) Rubinstein, I.; Shtilman, L. Voltage against current curves of cation exchange membranes. *J. Chem. Soc., Faraday Trans. II* **1979**, *75*, 231−246.
(52) Rubinstein, I.; Zaltzman, B. Electro-osmotically induced convection at a permselective membrane. *Phys. Rev. E* **2000**, *62*, 2238−2251.
(53) Rubinstein, I.; Zaltzman, B.; Lerman, I. Electroconvective instability in concentration polarization and nonequilibrium electro-osmotic slip. *Phys. Rev. E* **2005**, *72*, 011505.
(54) Ben, Y.; Chang, H.-C. Nonlinear Smoluchowski slip velocity and micro-vortex generation. *J. Fluid Mech.* **2002**, *461*, 229−238.
(55) Leinweber, F. C.; Tallarek, U. Nonequilibrium electrokinetic effects in beds of ion-permselective particles. *Langmuir* **2004**, *20*, 11637−11648.
(56) Rubinstein, S. M.; Manukyan, G.; Staicu, A.; Rubinstein, I.; Zaltzman, B.; Lammertink, R. G. H.; Mugele, F.; Wessling, M. Direct observation of a nonequilibrium electro-osmotic instability. *Phys. Rev. Lett.* **2008**, *101*, 236101.
(57) Levich, V. G. *Physicochemical Hydrodynamics*; Prentice-Hall: New York, 1962.
(58) Maletzki, F.; Rösler, H.-W.; Staude, E. Ion transfer across electrodialysis membranes in the overlimiting current range: stationary voltage current characteristics and current noise power spectra under different conditions of free convection. *J. Membr. Sci.* **1992**, *71*, 105−115.
(59) Karthika, P.; Rajalakshmi, N.; Dhathathreyan, K. S. Function-alized exfoliated graphene oxide as supercapacitor electrodes. *Soft Nanosci. Lett.* **2012**, *2*, 59−66.
(60) Joshi, R. K.; Carbone, P.; Wang, F. C.; Kravets, V. G.; Su, Y.; Grigorieva, I. V.; Wu, H. A.; Geim, A. K.; Nair, R. R. Precise and ultrafast molecular sieving through graphene oxide membranes. *Science* **2014**, *343*, 752−754.
(61) Ehlert, S.; Hlushkou, D.; Tallarek, U. Electrohydrodynamics around single ion-permselective glass beads fixed in a microfluidic device. *Microfluid. Nanofluid.* **2008**, *4*, 471−487.

(62) Konkena, B.; Vasudevan, S. Understanding aqueous dispersibility of graphene oxide and reduced graphene oxide through pKa Measurements. *J. Phys. Chem. Lett.* **2012**, *3*, 867−872.
(63) Hasan, S. A.; Rigueur, J. L.; Harl, R. R.; Krejci, A. J.; Gonzalo-Juan, I.; Rogers, B. R.; Dickerson, J. H. Transferable graphene oxide films with tunable microstructures. *ACS Nano* **2010**, *4*, 7367−7372.
(64) Bai, H.; Li, C.; Wang, X.; Shi, G. On the gelation of graphene oxide. *J. Phys. Chem. C* **2011**, *115*, 5545−5551.
(65) Hummers, W. S., Jr.; Offeman, R. E. Preparation of graphitic oxide. *J. Am. Chem. Soc.* **1958**, *80*, 1339.